On the Effect of mixing Small Quantities of Cobalt with Brass

By

Daidzi Iitsuka

(Received April 26, 1929)

The present work has been undertaken with the object of finding out the effect of small quantities of cobalt when mixed with brass. It resulted in establishing the ternary equilibrium diagram in a corner, where the copper predominates in the ratio of 50%–100%, while zinc appears in the proportion of 0%–50% and cobalt, 0%–10%. Furthermore, some mechanical and corrosion tests were tried with a few new alloys which were considered technically important.

I The binary systems: Cu-Zn, Zn–Co and Cu–Co

For the Cu–Zn system, the author's own diagram[1] (Fig. 1), and for the Zn–Co system, Lewkonja's[2] (Fig. 2) were adopted not modified in any way. For the Cu–Co system, however, Sahmen's diagram[3] (Fig. 3) has to be modified, in so far as it concerns the curves for the primary crystallisation.

According to the author's experiment, copper and cobalt are not completely soluble in the molten state but form two liquid layers, the solubility-limits at a temperature a little higher than 1110°C being 3.5% Co on the copper side (=solution *d*) and probably 8% Cu on the cobalt side (=solution *b*). A series of cobalt-solid solutions separates out from the solution *d* on cooling till it goes into a peritectic reaction with the copper-rich melt at 1110°C. On cooling further, a series of copper-solid solutions is again forced

---

1 These Memoirs, A, **8**, 179 (1925)

2 Zs. f. anorg. Chem., **59**, 1 (1908)

3 *ibid.*, **57**, 293 (1907)

Fig. 1

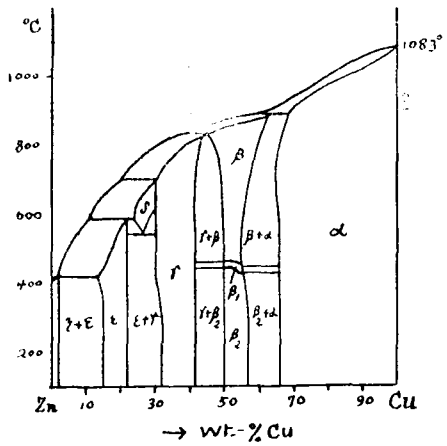

Fig. 2

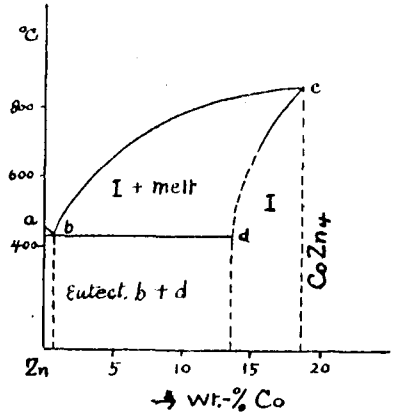

Fig. 3

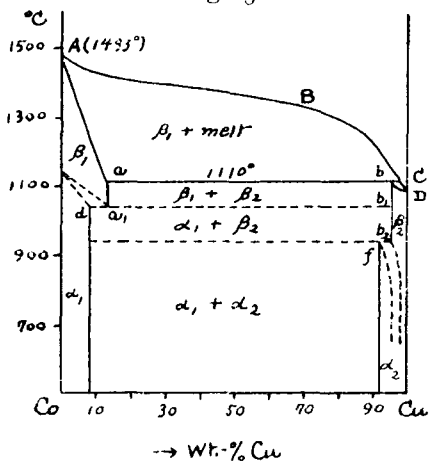

to crystallise till it reaches at last the copper-axis. According to Sahmen, this solid solution β_2 is destined to be transformed into α_2: such was however not found to be the case in the author's experiment. Fig. 4 is plotted mainly according to the author's own data, except that the details at the cobalt side are provisionally given in dotted lines, owing to the fact that the determinations with respect to those points are practically impossible.

II The ternary system: Cu–Zn–Co

An investigation of the ternary system Cu–Zn–Co within the narrow limit of 0.5%–5.0% Co to brasses with 70%, 60% and 55% Cu was attempt-

Fig. 4

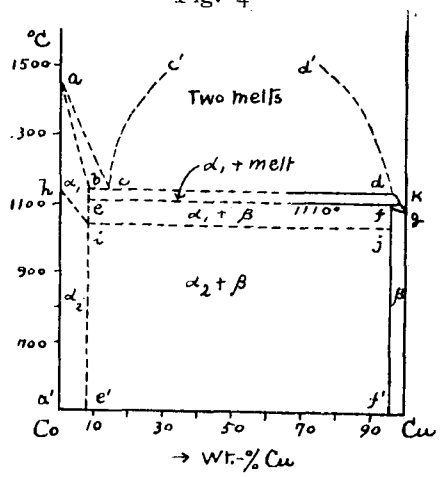

ed by Guillet[1] in 1920. The purpose of his investigation was not, however, to establish the ternary equilibrium diagram, but to find out the effect of cobalt on the mechanical properties and the microstructures of brass, and he concluded that cobalt has no favourable effect.

The present author, however, went on further in the limits of the composition, applied such means of investigation as thermal analysis, heat-treatments and microstructures, thereby being enabled to establish a part of the equilibrium diagram, and also to get a result differing from Guillet's in that the addition of some cobalt was found to be rather commendable in many cases.

Results of thermal analysis (Table III–X), heat-treatments and microstructures (Table XI), mechanical (Table XII) and corrosion tests (Table XIII) are each afterwards given in appropriate places.

The zinc and cobalt used as materials were both Kahlbaum's " pure " and the copper electrolytic. Changes of composition by volatilisation and oxidation were prevented as much as possible in this way, that the zinc was fused under molten sodium chloride in a porcelain crucible and kept slightly lower than its boiling point, and into it the copper and cobalt were alternately thrown in small pieces all the while being well stirred; thereupon the temperature was raised as much as would cause the mixture to come to a homogeneous solution. Furthermore, some of the alloys thus prepared, which are especially of technical importance, were analysed, the results of which

1 Rev. de Métallurgie, **17**, 494 (1920)

are given in Tables I and XII, inasmuch as the data given in Table II refer simply to the numbers of the mixed quantities.

On the basis of those data, the ternary equilibrium diagram, Fig. 5, was constructed, and its projection is shown in Fig. 6. The dotted lines there refer to the field boundaries at higher temperatures, while the full lines refer to those at ordinary ones. The projective diagram is divided into the following nine fields for the sake of illustration :—

1. *a'b'h'p'jk'a'*, 2. *b'c'h'b'*, 3. *c'c'h'f*,
4. *fh'p'g*, 5. *gp'n'i*, 6. *in'n'lq*,
7. *p'js'm'olu'n'p'*, 8. *x'lor'*, 9. *qlx'*.

Table I

No.	Cu %	Zn %	Co (diff.) %
119	99.14	0	0.86
115	95.17	0	4.83
107	81.04	0	18.96
13	91.07	7.73	1.20
15	89.43	7.77	2.80
16	88.09	8.14	3.77
105	70.26	9.69	20.05
68	74.89	24.61	0.50
71	74.03	24.39	1.58
61	72.18	24.88	2.94
88	63.72	29.18	7.10
33	62.12	35.69	2.19
101	57.08	35.72	7.20
90	50.74	29.71	19.55
74	51.97	45.37	2.66
25	57.01	41.43	1.56
26	51.21	44.88	3.91
111	51.84	45.69	2.47

Table II

No.	Cu %	Zn %	Co %
121	100	0	0
118	98	0	2
117	97	0	3
1	97	2	1
2	96	2	2
3	95	2	3
8	93	5	2
9	92	5	3
14	90	8	2
54	88	11	1
19	87	11	2

Table II continued

No.	Cu %	Zn %	Co %
76	84.5	15	0.5
77	84	15	1
78	83	15	2
79	82	15	3
92	79	18	3
67	79.5	20	0.5
64	79	20	1
65	77	20	3
102	75	23	2
63	74	25	1
69	71.5	28	0.5
47	71	28	1
46	70	28	2
70	69.5	30	0.5
53	69	30	1
43	68	30	2
48	67	32	1
40	66	32	2
116	96	0	4
120	90	0	10
4	94	2	4
5	93	2	5
99	92	2	6
6	90	2	8
7	85	2	13
98	91	5	4
10	90	5	5
97	89	5	6
11	88	5	7
12	85	5	10
96	87	8	5
17	86	8	6
18	82	8	10
20	85	11	4
94	84	11	5
21	83	11	6
22	81	11	8
23	79	11	10
103	83	13	4

Table II continued

No.	Cu %	Zn %	Co %
93	82	13	5
80	80	15	5
91	77	18	5
66	75	20	5
82	72	20	8
83	70	20	10
106	60	20	20
95	74	23	3
60	71	25	4
62	69	25	6
84	67	25	8
55	69	28	3
81	64	25	11
56	67	28	5
57	66	28	6
85	64	28	8
44	66	30	4
45	64	30	6
89	60	30	10
41	64	32	4
42	62	32	6
87	60	32	8
37	62	34	4
38	60	34	6
39	58	34	8
86	56	34	10
34	60	36	4
35	58	36	6
31	58	38	4
104	57	38	5
32	56	38	6
28	56	40	4
113	55	40	5
29	54	40	6
114	54	41	5
49	65	34	1
36	64	34	2
50	63	36	1
51	61	38	1

Table II continued

No.	Cu %	Zn %	Co %
30	60	38	2
52	59	40	1
27	58	40	2
58	56	41	3
72	57·5	42	0·5
59	57	42	1
24	54	45	1
109	51	45	4
73	54·5	45	0·5
112	50	46	4
110	51	47	2
75	54	42	4
108	53	42	5

Table III

No.	Liquidus °C	Solidus °C	Peritectic		Field & Structure
			°C	Sec.	
121	1083 (m.p. of Cu)				a'b'c'h'p'jk'a'—field. (8)
119	1093	1087	—	—	
118	?	?	1108	1	
117	?	?	1108	5	
1	1091	1084	—	—	
2	?	1088	1103	4	
3	?	1093	1101	4	
8	?	1076	1096	?	
9	?	1088	1097	2	
13	1079	1054	—	—	
14	?	1062	1088	3	
15	?	1066	1090	4	
54	1068	1035	—	—	
19	?	1052	1072	5	
76	1045	1006	—	—	
77	1050	1008	—	—	
78	?	1010	1055	?	
79	?	1016	1055	3	
92	?	1005	1035	2	
67	1007	973	—	—	

Table III continued

No.	Liquidus °C	Solidus °C	Peritectic		Field & Structure
			°C	Sec.	
64	1017	977	—	—	a'b'c'h'p'jk'a'—field. (α)
65	?	980	1029	?	
102	?	957	1005	?	
68	968	934	—	—	
63	970	940	—	—	
71	?	947	998	?	
69	955	915	—	—	
47	973	918	—	—	
46	975	922	—	—	
70	953	905	—	—	
53	955	910	—	—	
43	965	920	—	—	
48	950	—	917	2	
40	956	—	923	?	

Table IV

No.	Peritectic		Field & Structure
	°C	Sec.	
116	1108	7	e'd'c'h'f—field. (α+γ)
115	1110	5	
120	1109	3	
107	1110	2	
4	1100	3	
5	1102	4	
99	1100	?	
6	1103	?	
7	1101	?	
98	1095	3	
10	1095	3	
97	1095	2	
11	1095	2	
12	1096	2	
16	1090	4	
96	1090	3	
17	1090	3	
18	1092	?	

Table IV continued

No.	Peritectic		Field & Structure
	°C	Sec.	
105	1068	?	e'd'c'h'f—field. ($\alpha+\gamma$)
20	1070	4	
94	1070	2	
21	1070	?	
22	1072	?	
23	1070	?	
103	1063	2	
93	1062	?	
80	1053	4	
91	1032	3	
66	1025	3	
82	1022	3	
83	1017	?	
106	1007	2	
95	1008	3	
61	1003	5	
60	1002	3	
62	1000	2	
84	998	?	
81	984	?	
55	985	?	

Table V

No.	Liquidus (α) °C	Solidus (α) °C	Field & Structure
56	979	948	f'h'p'g—field. ($\alpha+\gamma$)
57	978	943	
85	977	940	
44	975	940	
45	973	935	
88	972	930	
89	970	928	
41	970	927	
42	967	924	

Table VI

No.	Liquidus (α) °C	Peritectic		Field & Structure
		°C	Sec.	
87	970	927	3	gp'n'i—field. (α+β+γ)
37	968	927	3	
38	963	928	3	
39	960	926	4	
86	958	927	7	
34	956	927	4	
35	951	928	5	
101	948	927	9	
31	945	928	9	
104	943	926	10	
32	940	927	10	
28	934	928	10	
113	932	927	10	
29	930	927	6	
90	965	927	6	

Table VII

No.	Liquidus (β) °C	Solidus (β) °C	Liquidus (α) °C	Peritectic		Field & Structure
				°C	Sec.	
114	—	—	930	927	8	in'u'lq—field. (α+β+γ)
75	927	918	—	—	—	
108	928	919	—	—	—	

Table VIII

No.	Liquidus (α) °C	Peritectic		Solidus (β) °C	Liquidus (β) C°	Field & Structure
		°C	Sec.			
49	945	915	4	—	—	p'js'm'olu'n'p'—field. (α+β)
36	953	922	3	—	—	
50	938	917	7	—	—	
33	945	923	6	—	—	
51	928	918	10	—	—	
30	937	923	8	—	—	
52	924	918	7	909	—	
27	925	922	2	915	—	
58	929	925	2	?	—	
72	910	907	4	897	—	
59	919	917	7	906	—	
74	920	918	4	912	—	
24	—	—	—	888	913	
25	—	—	—	893	916	

Table IX

No.	Liquidus °C	Solidus °C	Field & Structure
73	900	885	x'lor'—field. (β)
111	908	895	
110	905	883	

Table X

No.	Liquidus (β) °C	Solidus (β) °C	Field & Structure
109	918	900	q1x'—field. (α+β)
26	922	913	
112	910	890	

Fig. 5

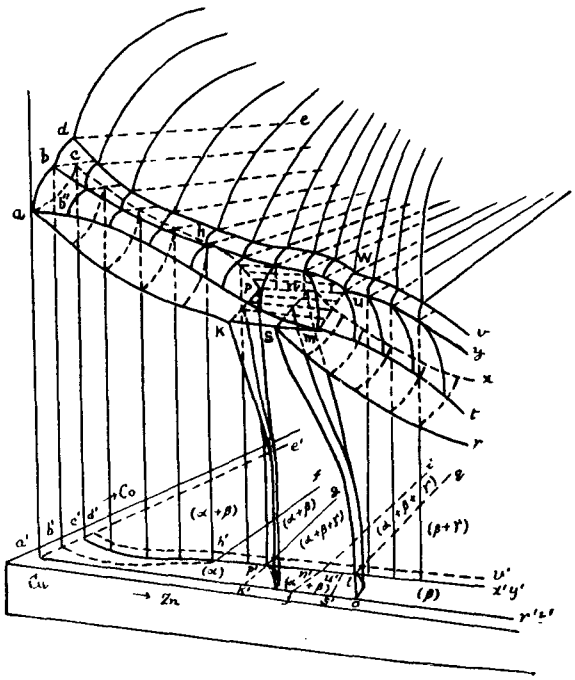

Fig. 6

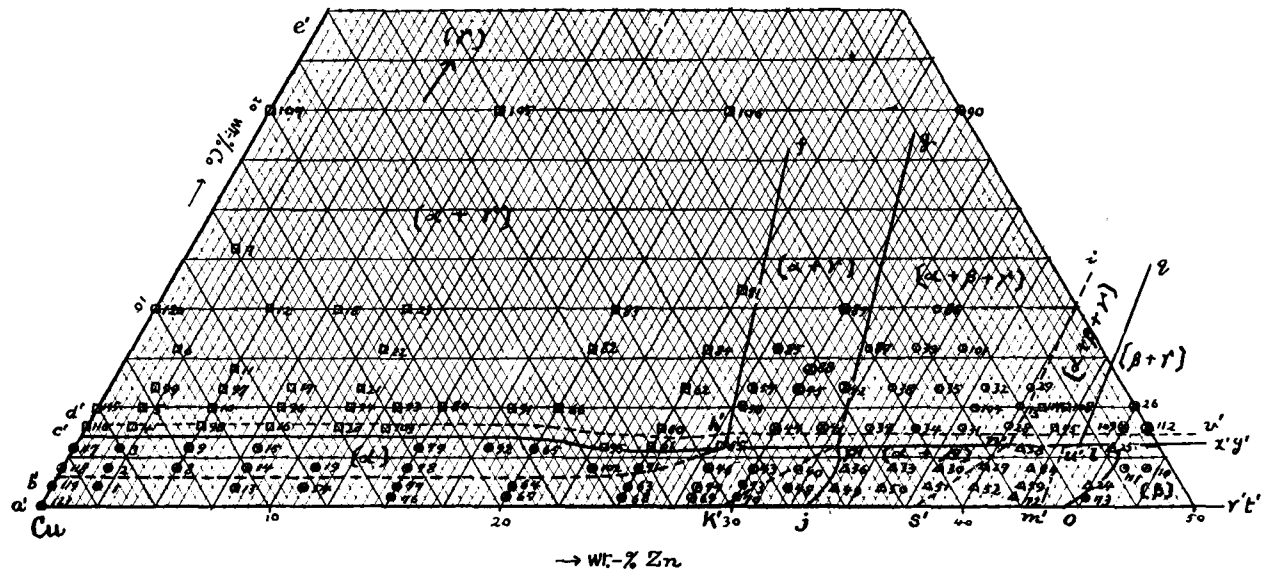

1 The field–$a'b'h'p'jk'a'$: structure α

The alloys in this field are all of the α-structure at room-temperature, as shown in Photo. I. The melt begins to separate out the α-crystals at the temperatures below those of the liquidus surface and ceases at the temperatures of the solidus-surface enclosing the field *ab''chpka*, where a space-curve *pk* shows the concentration of the saturated mixed crystals. The boundary-surface, *jkpp'*, which the α-field will form with the seventh field *p'js'm'olu'n'p'*, shows an inclination towards the right when the temperatures are lowered, so that the α-field will get widened at room-temperature in the limit of *p'jk'p'*, which consisted formerly of the bi-structure of α and β.

2 The field–$b'c'h'b'$: structure α

In this field a Co-rich ternary mixed crystal γ begins to separate out of the melt at the temperatures represented by a part of the liquidus-surface *dbhuvd*. The separation continues till the temperatures of the peritectic-surface *bchb* are reached ; at these temperatures the melt of *bh* and γ enter on a peritectic reaction on the withdrawal of heat, forming a saturated ternary mixed crystal α represented by a space-curve *ch* at the expense of all of γ. The melt now in equilibrium with α crystallises entirely at the temperatures of the solidus-surface *ab''chpka*. The structure of this field consists therefore generally of α, but according to the ratio of cooling velocities a skeleton-like structure is sometimes observed due to the peritectic reaction, as shown in Photo. 2.

3 The field–$e'c'h'f$: structure $\alpha+\gamma$

The field concerns the Cu-side, and the Co-side, being saturated, melts immiscibly and in equilibrium at high temperatures. On the fall of temperature, the Co-rich melt begins to separate out the Co-rich ternary mixed crystal γ, when it reaches a space-surface *edvw*, where the composition of the melt becomes so Cu-rich as indicated by the space-curve *dw*.

At this stage, the Co-rich melt disappears, while the Cu-rich homogeneous melt is left behind. On further cooling, the mixed crystal γ will be separated continuously from the melt till the melt finally takes the composition of the space-curve *bh*, where it goes on the withdrawal of heat into a peritectic reaction with the mixed crystal γ in order to form α as indicated by a space-curve *ch*. This reaction comes to end with the disappearance of the melt.

The structure consists therefore of a mixture of α and γ, as may be seen from Photo. 3, where the bright star-like crystals γ are scattered on the ground of α.

4 The field-*fh'p'g*: structure $\alpha+\gamma$

Two immiscible liquids coexist at high temperatures in this field as in the former one. As soon as the temperatures fall to a space-surface *edw*, a Co-rich crystal γ being separated out of the Co-rich melt, the remainder of the liquid becomes by and by Cu-richer, so that it falls finally to the compositions indicated by the space-curve *dw* where the Co-rich liquid disappears.

On cooling further, the melt continues to separate out the Co-rich mixed crystal γ till it reaches the space-curve *hu*. When the temperatures still fall underneath the space-curve *hu*, the Cu-saturated mixed crystal α separates out along the space-curve *hp*, whereupon the melt becoming Cu-less tends to move along the curve *hu* towards the right. In this way, there exists an equilibrium, as represented by a vertical plane *phunp*, between the α-crystal along the curve *hp* and the melt along the curve *hu*. Below the temperatures of the curve *hp*, the alloys should all be solid. In so far as elucidated, we may see that the structure of the alloys in this field must also consist of α and γ (Photo. 4), but that the α is of primary nature and not a product of a peritectic reaction as in the third field.

5 The field-*gp'n'i*: structure $\alpha+\beta+\gamma$

One of the two liquids immiscible at high temperatures, namely the Co-rich one, now commences to deposit γ at the temperatures of the space-surface *edw*, as the result of which the liquid tends to become Cu-rich till it acquires at last the compositions of the curve *dw*. On further cooling, it will cause the deposition of the Co-rich crystals along the space-surface *wdbhuw*, and when the temperatures are so low as to touch the space-curve *hu*, the solid phase in equilibrium with the melt will be α along the curve *hp*, while the remainder of the melt will move from *h* to *n* along the curve *hu*. Finally, when the solid phase α stands in equilibrium with the liquid *n*, the withdrawal of heat will result in a peritectic reaction at *n* so as to form a new ternary mixed crystal β.

The structure of the alloys in this field must therefore consist of three phases α, β and γ. (See Photo. 5)

6 The field-*in'u'lq* : structure $\alpha+\beta+\gamma$

On separating γ, the remainder of the melt will finally reach the curve *huy*. A further solidification of the melt must then go on differently either along the curve *hu* (1) or along the curve *uy* (2) :—

1) On being further cooled, the crystal α along the curve *hp* will be separated from the melt *hu* at the same rate as the remainder of the liquid becomes Cu-less. At temperatures so low as the line *pnu*, the Cu-saturated α-crystal (nominated *p*) will enter into a peritectic reaction with the melt *u* so as to give a new solid phase β (nominated *n*). On being lowered temperatures below the space-line *nu*, the composition of β will move along the space-curve *nx* and that of the melt along the space-curve *uy*. At the temperatures of *nx*, all comes to solidify at the expense of the melt.

2) In so much as the crystal β of the space-curve *nx* will be deposited along the decreasing temperatures, the remainder of the melt will change its composition along *uy*, and at the temperatures of the space-curve *nx* all will come to solidify.

As explained, the alloys solidify in both cases to a mixture of β and γ. The structure is, however, changed from the temperatures lower than the space-surface *osnl* by the segregation of α from β, so that the alloys in this field will show a triple structure consisting of α, β and γ at room-temperatures.

7 The field-*p'js'm'olu'n'p'* : structure $\alpha+\beta$

At the temperatures of the liquidus-surface *hum*, the melt separates α as primary crystals, and this will cause the composition on the space-surface *hum* to vary towards the right side, so as to reach the space-line *mu*. Here there takes place a peritectic reaction between α (along the space-line *pk*) and the melt (along the space-line *mu*), as the concecquence of which we have β (along the space-line *sn*). The ternary peritectic-surface spreads over as far as shown by the symbol *pksmunp*, and it is the continuity of the binary peritectic-line *ksm* in the Cu–Zn system. Two crystals α and β appear therefore in this field as the structural elements, as shown in Photo. 6.

The reguli having the compositions limited by the liquidus-surface *muh* and the solidus-surface *msnum* separate β only at the temperatures between those of the solidus-surface *rsnx* and of the boundary-surface *osnl*, and beneath the latter all the β segregates α owing to its change in solubility, so that the alloys will show anywhere a binary structure at room-temperatures.

8 The field-*x'lor'*: structure β

The alloys in this field begin to separate β represented by the space-surface *xnsr* at the temperatures of the liquidus-surface *yumt*, the composition of the residual liquid being thereby changed according to the space-surface *yumt*. The solidification is completed at the concave surface *rsnx*. The structure of the alloys is therefore β. (Photo. 7)

The boundary-surface *osnl* runs obliquely downwards and therefore limits the β-field wider at higher temperatures, which is a result following from the fact that β has a greater solubility for α at higher temperatures under the space-surface *rsnx*. For example, the alloy No. 25 (57.01% Cu, 41.43% Zn and 1.56% Co) takes the β-structure on quenching at 800°C (Photo. 8), while it consists of α and β when slowly cooled (Photo. 9). All other details are given in Table XI.

Table XI

No.	Quench. Temp. & Its Structure						
52	900° β	850° α+β	700° α+β	600° α+β	500° α+β		
27	910° α+β	850° α+β	650° α+β	500° α+β			
58	950° α+β+melt	920° α+β	900° α+β	750° α+β	550° α+β		
72	920° α+β+melt	900° β	850° β	800° α+β	750° α+β	600° α+β	500° α+β
59	900° β	850° β	800° α+β	780° α+β	750° α+β	700° α+β	600° α+β
74	900° β	850° β	820° α+β	750° α+β	700° α+β	550° α+β	
24	850° β	820° β	800° β	750° β	700° α+β	600° α+β	550° α+β
25	850° β	800° β	750° β	700° α+β	600° α+β	550° α+β	
73	800° β	700° β	600° β	500° β			
111	850° β	800° β	700° β	640° β	550° β		

9 The field-*qlx'*: structure $\beta+\gamma$

Depositing γ at falling temperatures, the Co-side liquid in equilibrium changes its composition till it reaches at last the space-curve *wv*, where the equilibrium comes to end. Down from these temperatures, the residual liquid still continues to give out γ along the liquidus-surface *vwuy* till it reaches finally the space-curve *uy*. Hereupon, the melt begins, on the withdrawal of heat, to deposit β (along the space-curve *nx*) vertically down

along the space-plane *xnuy*. The solidification now concludes at the space-curve *nx*.

The structure of the alloys consists therefore of β and γ. (Photo. 10)

Sectional Diagrams of the Equilibrium-Model

Five sectional diagrams were obtained by cutting the equilibrium-model with vertical planes, OP, QR, ST, VW and XY as shown in Fig. 7. These are given in Fig. 8–12.

Fig. 7

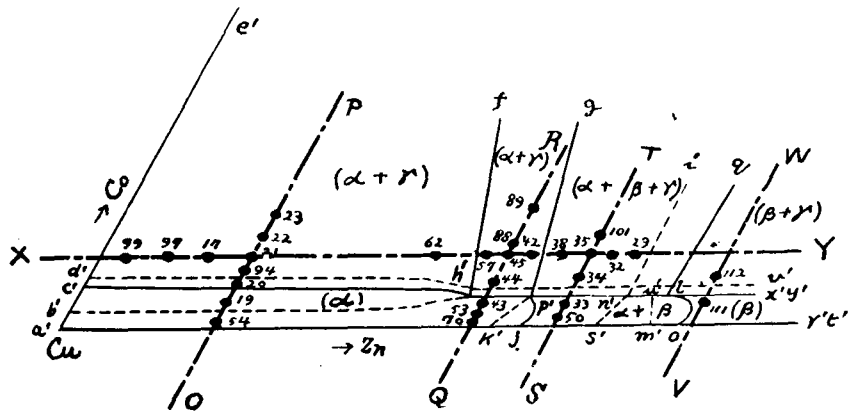

Fig. 8

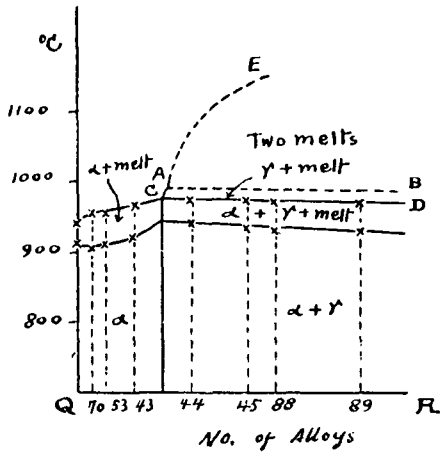

Fig. 9

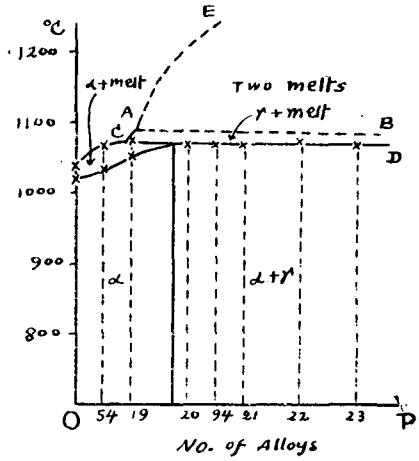

Fig. 10

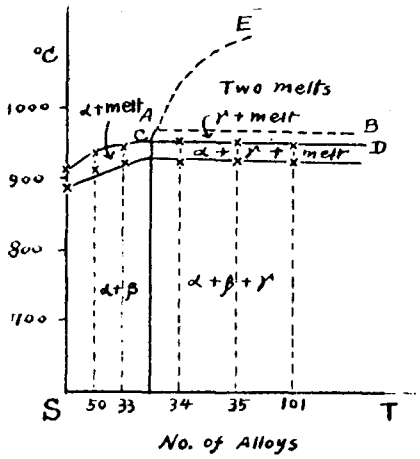

Fig. 11

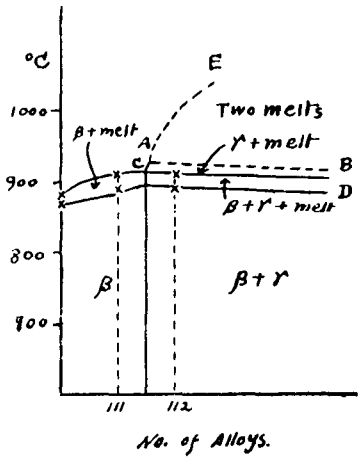

Fig. 12

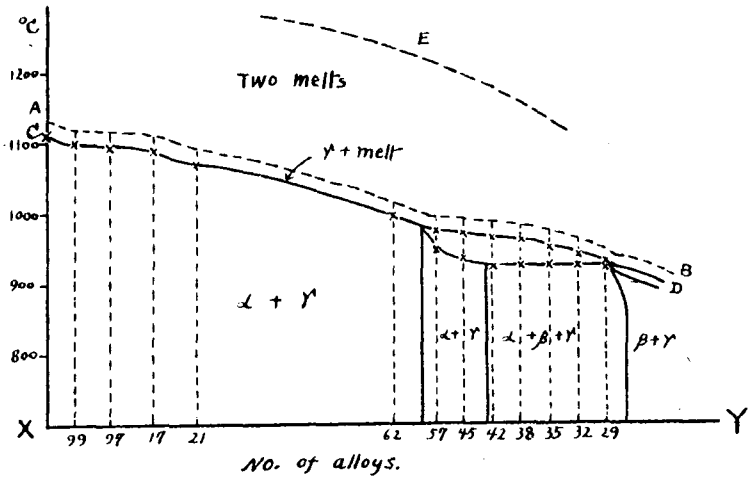

The dotted line AE shows a part of the conjugate line representing the equilibrium-state between the two immiscible liquids. Their temperatures of equilibrium are not to be measured.

The dotted horizontal line AB indicates the beginning temperatures of primary crystallisation of γ in the Co-rich melt.

No thermal effect due to γ is clearly to be perceived, because the Co-content is too small in the limits of our determination.

Mechanical Tests

Test bars of definite compositions, cast in sand moulds, were machined down to the required dimensions, as shown in Fig. 13. After annealing for one hour, in order to secure uniformity in composition, they were subjected to tests for ultimate strengths and elongation percentages. The results are given in Table XII.

Fig. 13

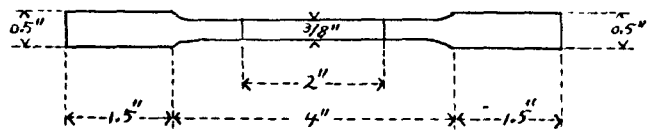

Table XII

Mark	Composition—%			Ultimate Strength Tons per sq. in.	Elongation Per Cent on 2 in.
	Cu	Zn	Co (diff.)		
A	60.82	39.04	—	4.09	25.00
E	59.47	39.44	1.09	4.15	28.13
B	59.79	38.08	2.13	4.41	28.13
C	59.61	37.29	3.10	4.20	25.00
D	59.02	37.07	3.91	3.64	18.75
F	70.50	29.69	—	2.89	43.75
I	71.85	27.01	1.14	3.01	34.37
G	72.07	26.08	1.85	3.25	31.25
H	70.87	26.39	2.74	2.92	13.12

Addition of 1%–2% of Co raises the tensile strength of the F-alloy (70 : 30-brass) at the expense of a slight amount of elongation, and both the strength and the elongation of the A-alloy (60 : 40-brass).

These facts lead us to the generalisation, that β-brass is improved in all its mechanical properties by addition of Co, while α-brass is improved in strength but not in elongation. Reference shonld be made to Table XII, alloys I, G and H. We see, therefore, that A-alloy, on the addition of Co,

will gain much more elongation in α than it will lose in β, which results in the improvement of its properties as a whole. Alloys E and B, Table XII, are examples of improved brasses.

Corrosion Tests

A series of experiments was carried out for corrosion in sea-water with several Co-containing 60 : 40-brasses, the compositions of which are given in Table XII.

These alloys were immersed in artificial sea-water with 5% NaCl by weight, which was kept nearly constant at 100°C in a water-bath. After 50 and 100 days, they were taken out of the sea-water, scrubbed carefully with a brush, washed with hot water, dried at 200°C and then weighed. Losses in weight were recalculated for grams per 5 cm^2.

The details of the researches are given in Table XIII, and their purport is this :—

60 : 40-brass with 3%–4% Co added is more resistant against sea-water than simple brass. The compositions of the best alloys are marked C and D in the Table.[1]

Table XIII

Mark	Surface area of alloy $cm.^2$	Original Wt. of alloy gr.	Wt. after 50 days gr.	Wt. after 100 days gr.	Final loss in Wt. gr.	Loss in Wt. per 5 $cm.^2$ gr.
A	3.77	5.8120	5.7712	5.7450	0.0676	0.0888
E	3.77	5.2013	5.1687	5.1500	0.0513	0.0680
B	2.76	3.2943	3.2759	3.2647	0.0296	0.0536
C	2.43	2.7550	2.7457	2.7368	0.0182	0.0374
D	2.97	2.8265	2.8180	2.8113	0.0152	0.0256
T	2.76	3.3058	3.2863	3.2728	0.0330	0.0598
Y	3.25	2.9080	2.8820	2.8725	0.0355	0.0546

In conclusion, the author wishes to acknowledge his indebtedness to Prof. M. Chikashige for his valuable suggestions throughout the course of the investigation.

1 Naval brass, Y- and T-alloys, does not show any superiority over our cobalt-brass as co-tabulated in the Table.

Y-alloy: 59.07% Cu, 38.88% Zn, 2.05% Sn.
T-alloy: 59.61% Cu, 39.42% Zn, 0.97% Sn.

Plate I

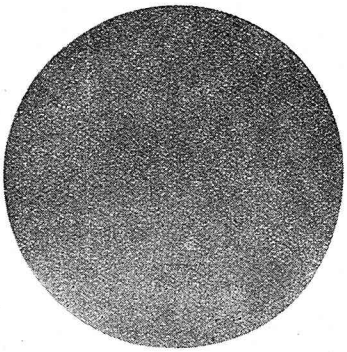

Photo. 1. No. 68–alloy.
Cu 74.89%, Zn 24.61%, Co 0.50%.
As Csat. ×120.

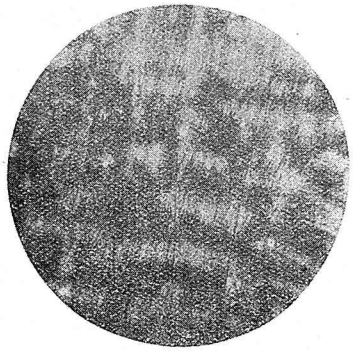

Photo. 2. No. 71–alloy.
Cu 74.03%, Zn 24.39%, Co 1.58%.
As Cast. ×120.

Photo. 3. No. 61–alloy.
Cu 72.18%, Zn 24.88%, Co 2.94%.
As Cast. ×120.

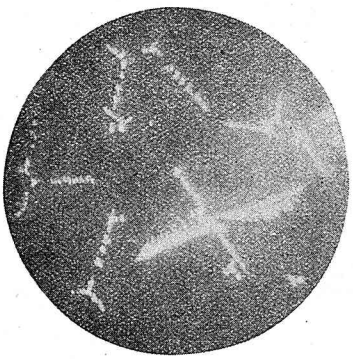

Photo. 4. No. 88–alloy.
Cu 63.72%, Zn 29.18%, Co 7.10%.
As Cast. ×120.

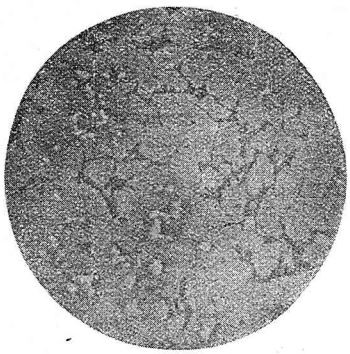

Photo 5. No. 101–allor.
Cu 57.08%, Zn 35.72%, Co 7.20%.
As Cast. ×120.

Photo. 6. No. 33–alloy.
Cu 62.12%, Zn 35.69%, Co 2.19%.
As Cast. ×120.

Plate II

Photo. 7. No. 111-alloy.
Cu 51.84%, Zn 45.69%, Co 2.47%.
As Cast. ×120.

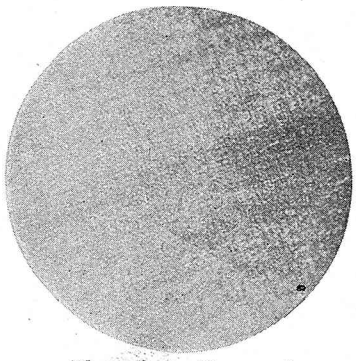

Photo. 8. No. 25-alloy.
Cu 57.01%, Zn 41.43%, Co 1.56%.
Quench. at 800°C. ×120.

Photo. 9. No. 25-alloy.
(The same as Photo. 8)
As Cast. ×120.

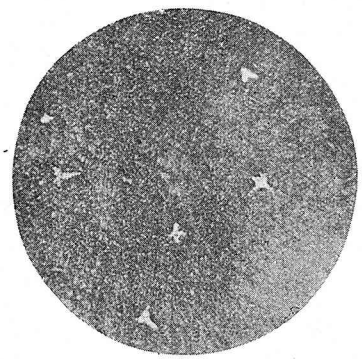

Photo. 10. No. 26-alloy.
Cu 51.21%, Zn 44.88%, Co 3.91%.
As Cast. ×120.